Letter to the Editor

Magnetic helicity and energy budgets of jet events from an emerging solar active region

A. Nindos[1], S. Patsourakos[1], K. Moraitis[1], V. Archontis[1], E. Liokati[1], M. K. Georgoulis[2,3], and A. A. Norton[4]

[1] Section of Astrogeophysics, Department of Physics, University of Ioannina, 45110, Greece.
  e-mail: `anindos@uoi.gr`
[2] The Johns Hopkins University Applied Physics Laboratory, Laurel, MD, 20723, USA
[3] Research Center for Astronomy and Applied Mathematics, Academy of Athens, Athens, 11527, Greece
[4] HEPL Solar Physics, Stanford University, 94305-4085, Stanford, CA, USA

ABSTRACT

Using photospheric vector magnetograms obtained by the Helioseismic and Magnetic Imager on board the Solar Dynamic Observatory and a magnetic connectivity-based method, we compute the magnetic helicity and free magnetic energy budgets of a simple bipolar solar active region (AR) during its magnetic flux emergence phase which lasted ~47 hrs. The AR did not produce any coronal mass ejections (CMEs) or flares with an X-ray class above C1.0 but it was the site of 60 jet events during its flux emergence phase. The helicity and free energy budgets of the AR were below established eruption-related thresholds throughout the interval we studied. However, in addition to their slowly-varying evolution, each of the time profiles of the helicity and free energy budgets showed discrete localized peaks, with eight pairs of them occurring at times of jets emanating from the AR. These jets featured larger base areas and longer durations than the other jets of the AR. We estimated, for the first time, the helicity and free magnetic energy changes associated with these eight jets which were in the ranges of $0.5 - 7.1 \times 10^{40}$ Mx^2 and $1.1 - 6.9 \times 10^{29}$ erg, respectively. Although these values are one to two orders of magnitude smaller than those usually associated with CMEs, the relevant percentage changes were significant and ranged from 13% to 76% for the normalized helicity and from 9% to 57% for the normalized free magnetic energy. Our study indicates that occasionally jets may have a significant imprint in the evolution of helicity and free magnetic energy budgets of emerging active regions.

Key words. Sun: magnetic fields - Sun: flares - Sun: photosphere - Sun: corona

1. Introduction

Solar jets are collimated ejections of plasma that is launched outward along magnetic field lines. They occur prolifically in diverse environments such as coronal holes, the quiet Sun, and active regions (ARs) and are observed in different wavebands, most notably soft X-rays, EUV, and Hα, in the latter case being called surges (see reviews by Raouafi et al. 2016; Shen 2021; Schmieder et al. 2022, and references therein).

Jets are frequently associated with photospheric magnetic flux emergence or/and cancellation, as well as with signatures of impulsive release of energy such as micro-flaring activity at their bases (in what follows we use the term "jet base" to denote the structure in the EUV images from which the spire of the jet appears to emanate). These observations inspired a variety of numerical models in which jets result from magnetic reconnection between emerged magnetic field and the preexisting open magnetic field lines (e.g. Shibata et al. 1992; Yokoyama & Shibata 1995, 1996; Archontis & Hood 2008, 2012, 2013). Sometimes jets appear in conjunction with the eruption of mini filaments (e.g. Sterling et al. 2015, 2016) which motivated Wyper et al. (2017, 2018) to suggest that the material is ejected via a breakout mechanism.

There is a tradition of studying energetic magnetic phenomena in terms of their magnetic free energy (i.e. the term of the magnetic energy that is due to electric currents) and helicity (i.e. a measure of the twist, writhe, and linkage of the magnetic field

lines) budgets. Older (e.g. see Pevtsov et al. 2014, and references therein) and more recent (e.g. Liokati et al. 2022, 2023; Liu et al. 2023; Sun et al. 2024) results indicate that active regions (ARs) tend to produce eruptive flares (i.e. flares accompanied with coronal mass ejections, CMEs) when they accumulate significant budgets of both magnetic free energy and helicity. Furthermore some studies (e.g. Pariat et al. 2017; Thalmann et al. 2019; Gupta et al. 2021) indicate that the ratio of the magnetic helicity of the current-carrying field to the total magnetic helicity (named helicity index by these authors) is a reliable eruptivity proxy, whereas total magnetic energy and helicity are not.

Contrary to flares and CMEs, there is only a small number of publications discussing how the occurrence of jets is related to the helicity budget of their source regions. Numerical experiments (see Linan et al. 2018; Pariat et al. 2023) indicate that jet-producing simulations contain higher values of both free magnetic energy and helicity than the ones with no eruption and no jet. More importantly, it was found that the jet may occur when the helicity index attains its maximum value. As far as observations are concerned, Green et al. (2022) monitored the evolution of the helicity index in a large emerging eruptive active region and found that some major jets occurred at time intervals when the helicity index obtained large values.

In this Letter we present the evolution of magnetic helicity and free magnetic energy in an AR that produced several jet events during its flux emergence phase. We show, for the first
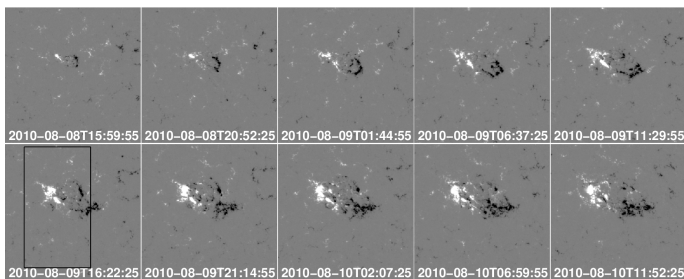
Fig. 1: Selected HMI line-of-sight magnetograms showing the evolution of the photospheric magnetic field in AR11096. In each image the field of view is 205″×205″. The black box shows the area that is displayed in Fig. A.1.

time with such clarity, that several of these jets occurred at times when both magnetic helicity and free energy showed distinct localized peaks and calculate the helicity and free magnetic energy changes associated with these jets.

2. Observations and data reduction

In this Letter we study emerging AR NOAA 11096. The morphological evolution of its photospheric magnetic field was studied using line-of-sight magnetograms from the Helioseismic and Magnetic Imager (HMI) on board the Solar Dynamics Observatory (SDO). The magnetic helicity and free magnetic budgets of the AR were calculated using HMI vector magnetograms. More specifically, we used the "hmi.sharp_cea_720s_dconS" data series which provides Lambert cylindrical equal-area (CEA) projections of the photospheric magnetic field vector (Bobra et al. 2014) that were corrected for scattered light (Couvidat et al. 2016; Norton et al. 2018). The correction did not modify the morphology of the AR field captured by the magnetograms but it increased the average total field strength across the field of view by a factor which varied during the observations from 1.19 to 1.41. The pixel size of the magnetograms was equivalent to about 360 km at disk center while the cadence of the vector field image cubes was 12 min.

At each timestamp we computed the instantaneous free magnetic energy and helicity budgets using the connectivity-based (CB) method of Georgoulis et al. (2012). The input of this method is a single vector magnetogram which is partitioned to yield a connectivity matrix populated by the magnetic flux associated with connections between partitions of opposite polarities. This collection of connections is treated as an ensemble of force-free flux tubes each with known footpoints, force-free parameter, and flux. For the system of these flux tubes the method delivers lower-limit estimates of their free magnetic energy and helicity.

The results from the CB method were compared with results from the flux-integration (FI) method: in it the magnetic helicity and energy fluxes across the photospheric boundary are computed. The inputs of this method are the normal and tangential components of the photospheric magnetic field as well as the cross-field velocity field at the photosphere (e.g. Kusano et al. 2002). Details about the computational procedure are given in Liokati et al. (2022).

The jets associated with the AR were identified in 211 Å images from the Atmospheric Imaging Assembly (AIA) telescope onboard SDO. This AIA channel is sensitive to 2 MK plasmas. Since it is unlikely that tiny, short-lived jets have any impact on the magnetic helicity and energy budgets of the AR, we degraded the cadence of our AIA datacube from 11 s to 2 min.

3. Results

The emergence of AR11096 started on 08 August 2010 11:00 UT (heliographic coordinates N22W08) in an area without pre-existing ARs (see Fig. 1 for characteristic snapshots). Inspection of 211-Å AIA movies indicate that the AR produced several jets, most of which occurred during its emergence phase. Therefore we limited our calculations to the flux emergence phase of the AR which (as was found from the time profile of the unsigned flux of the photospheric field) lasted ~47 hours.

Fig. 1 indicates that AR11096 was a simple bipolar AR. The AR produced neither CMEs nor flares with an X-ray class above C1.0 (see Liokati et al. 2022, and also the time profile of the 211-Å flux from the AR in Fig. 2(a)). During the interval we studied, several jets emanated from the AR, most of them from its eastern part (see Appendix A). We identified 60 jets which is probably a lower limit because the cadence of the AIA data we used was 2 min. Characteristic snapshots of major jets hosted by the AR are given in Fig. A.1.
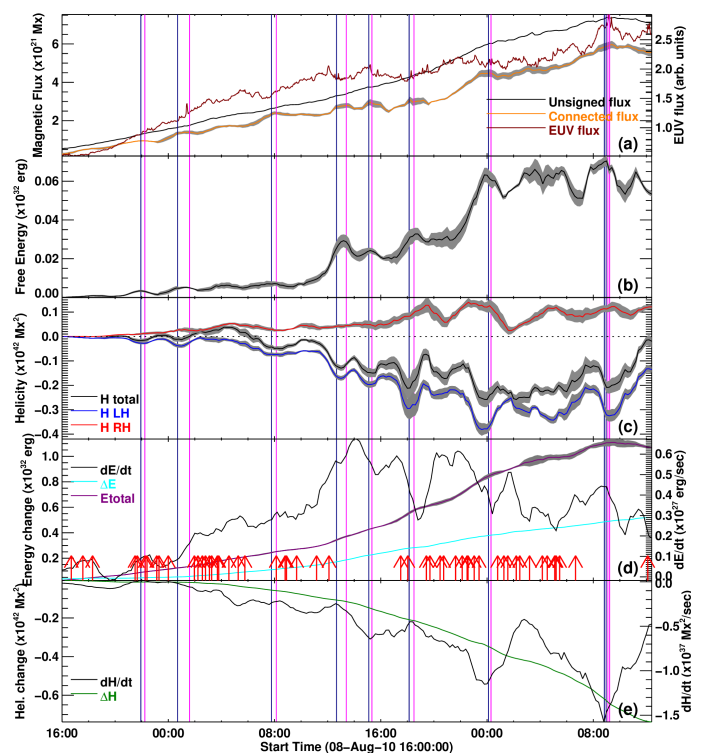

Fig. 2: Evolution of magnetic properties of AR11096. (a) Unsigned magnetic flux, unsigned connected magnetic flux used in the CB method, and EUV flux of the AR resulted from AIA's 211 Å channel (black, yellow, and maroon curves, respectively). (b) Free magnetic energy. (c) Net, left-handed, and right-handed helicity (black, blue, and red curves, respectively). (d) Total magnetic energy from the CB method, magnetic energy injection rate from the FI method and the corresponding accumulated magnetic energy (purple, black, and cyan curves, respectively). (e) Helicity injection rate from the FI method and the corresponding accumulated helicity (black and green curves, respectively). Vertical dark blue and pink lines show the start and end times of major jet events while arrows indicate the start time of the remaining jets of the AR. Error bars are indicated by the gray bands.

In Fig. 2 we give the time profiles of the free magnetic energy (E_f, panel b) and magnetic helicity (panel c) of the AR. In order to evaluate the long-term evolution of the magnetic energy and helicity all pertinent curves in this Letter are 48-min averages of the actual curves. Panels (b) and (c) indicate that both the free magnetic energy and net helicity curves exhibit slowly varying evolutionary patterns that are consistent with the evolution of both the unsigned magnetic flux, Φ, of the AR and the so-called connected flux, Φ_{conn} (i.e. the magnetic flux that populates the connectivity matrix employed by the CB-method, see Georgoulis et al. 2012).

The helicity curves (panel c) show that for most of the time interval we studied the net helicity is negative in agreement with the hemispheric helicity rule (Pevtsov et al. 1995); there is only a ~5-hour intrusion of positive net helicity starting at about 09 August 01:40 UT. Therefore it is not a surprise that the net helicity curve by and large follows the evolution of the negative helicity curve (correlation coefficient of 0.92).

The evolution of the injection rates of magnetic energy, dE/dt, and helicity, dH/dt, from the FI method as well as the resulting accumulated quantities (ΔE and ΔH, respectively) are given in panels (d) and (e) of Fig. 2. A direct comparison between the results from the CB-method and the results from the FI-method is not possible (see the discussion in Thalmann et al. 2021; Liokati et al. 2023). However, Fig. 2 indicates that there is a very good resemblance between the evolution of ΔE and the evolution of the total magnetic energy, E_{tot}, derived from the CB method (correlation coefficient of 0.96). The correlation coefficient between ΔH and the net helicity from the CB-method is 0.75, i.e. rather strong but weaker than that of the ΔE-E_{tot} pair. Furthermore, comparisons of the maximum values of the pertinent budgets derived by the two methods reveal differences of factors of 2.2 to 2.9 (these comparisons are meaningful because the starting value of both methods is close to zero). We repeated the calculations of the E_f and H budgets by the two methods after we degraded the resolution of the magnetograms to 2″. The new curves largely preserve the jet-related local peaks while the differences between the two methods decrease by fac-

tors of 1.1-1.3. This behavior is consistent with the findings by Wang et al. (2022). However, we note that the interpolation of the vector field data may influence the solenoidality of the field and the quality of azimuth disambiguation.

The free magnetic energy and helicity budgets of the AR are always clearly below reported thresholds for the occurrence of major flares; compare the values appearing in panels (b) and (c) of Fig. 2 with the thresholds of 4×10^{31} erg and 2×10^{42} Mx^2, respectively, established by Tziotziou et al. (2012). The accumulated budgets of ΔE and ΔH resulting from the FI-method (see panels (d) and (e) of Fig. 2) are also lower than the corresponding thresholds established by Liokati et al. (2022) (2×10^{32} erg and 9×10^{41} Mx^2, respectively) despite the fact that the data used by Liokati et al. (2022) were not corrected for scattered light.

The slowly-varying trends of the free magnetic energy and helicity budgets are paired with shorter localized peaks (see Fig. 2(b, c)). In eight cases these peaks are synchronized with jets produced in the AR. This is evident in Fig. 2 where the start and end times of major jet events produced in the AR are marked by dark blue and pink vertical lines, respectively. The localized peaks associated with the occurrence of jets appear co-temporally in the free magnetic energy, net helicity, H, and left-handed helicity (H_{LH}) curves. With the probable exception of the seventh event, their signature is not prominent in the right-handed helicity (H_{RH}) curve (that is, the minority sense of helicity). Furthermore, all the E_f-H localized peaks occurring in conjuction with jets stand out beyond error bars (the latter are indicated by the gray bands of Fig. 2 and result from the standard deviations of the moving five-point averages of the pertinent curves; see Moraitis et al. 2021; Liokati et al. 2023).

In Fig. 2 there are nine pairs of colored vertical lines corresponding to eight localized peaks (hereafter referred to as events 1-8) in each of the E_f, H, and H_{LH} curves. The mismatch comes from the fact that event 8 takes place during the occurrence of two temporally overlapping jets (see bottom right panel of Fig. A.1). Most of these localized E_f and H peaks occur either around the start time of a major jet (peaks 1, 3, and 5) or between the start and end time of a major jet (events 2, 4) while for the others, small temporal offsets can be registered between the $E_f - H$ peaks and the interval of occurrence of the jet. These offsets were on the order of 12-24 min and consequently they were barely resolved because the cadence of the magnetograms was 12 min.

Panels (d) and (e) of Fig. 2 indicate that the occurrence of events 1-8 was not associated with any prominent signature in the ΔE and ΔH curves. However, the dE/dt curve shows local peaks associated with events 3, 4, and 8 while the dH/dt curve shows absolute value local peaks associated with events 3, 5, 7, and 8. Using the binomial distribution test we found that the likelihood for incidental peak matchings between the curves from the two methods is 11% and 24% for the magnetic energy and helicity, respectively.

In Fig. 3 we present the evolution of the ratio of E_f to the total magnetic energy, E_f/E_{tot}, as well as the connected-magnetic-flux normalized helicities (H/Φ_{conn}^2, H_{RH}/Φ_{conn}^2, H_{LH}/Φ_{conn}^2). The values of these curves are a factor of ~2 lower than those associated with the two large eruptive ARs studied by Liokati et al. (2023). However, the normalized parameters of the free energy and helicity exhibit well-defined local peaks that are associated with jet events 1-8. We cannot test the behavior of the helicity index (see Sect. 1) because the CB method does not allow the decomposition of the total helicity to the parameters required for its calculation (the helicity index is calculated on 3D-inferred helicity estimation, hence the CB method is not designed to compute it).
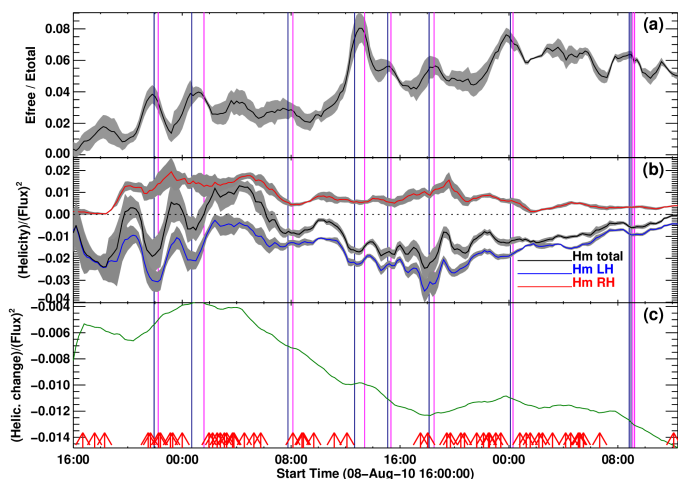

Fig. 3: Evolution of normalized magnetic quantities for AR11096. (a) Ratio of the free magnetic energy to the total magnetic energy. (b) Ratios of the net, left-handed, and right-handed helicity to the connected magnetic flux squared (black, blue, and red curves, respectively). (c) Ratio of the accumulated helicity from the FI method to the connected magnetic flux squared. Vertical lines and arrows are as in Fig. 2.

Returning to the CB budgets appearing in Fig. 2, the free magnetic energy and helicity changes (DE_f and DH, respectively) associated with the events 1-8 were calculated as the difference between the relevant localized peak and the value at the curve's point of inflection occurring just after the localized peak. The results appear in columns two and four of Table 1. The corresponding percentages of the normalized E_f and H losses (see Fig. 3) are given in columns three and five of Table 1. These percentages are all negative implying that free energy and helicity are taken away by the jets. The same behavior has been registered for large flares (e.g. Wang et al. 2023; Liokati et al. 2023). In this respect jets 1-8 can be considered as miniature eruptions.

In addition to the jet events that were associated with localized peaks in the free magnetic energy and helicity budgets of the AR, several other jets were also produced in the AR (their start times are denoted by the arrows in Figs. 2 and 3). The duration of these jets was short (see Fig. A.2(b)) and neither of them coincided with localized peaks appearing in both the E_f and H time profiles. We investigated how the former group of jets can be further distinguished from the latter. To this end, we calculated the apparent area of the bases (hereafter referred to as "area of the bases") of all jets that emanated from AR11096 (see Appendix A for details). The results appear in Fig. A.2(a) which indicates that on average the areas of the bases of the jets which are co-temporal with local peaks in the E_f-H budgets of the AR are statistically larger than the areas of those that have no significant imprint in the evolution of the E_f-H budgets.

4. Conclusions

In this paper we used the CB method (Georgoulis et al. 2012) to evaluate the free magnetic energy and helicity budgets of a small emerging AR. The AR was bipolar and during its emergence phase which lasted 47 hours produced no flares above C1.0-class or CMEs. However, we were able to identify by visual inspection of 211-Å movies 60 jets emanating from the AR.

Throughout the interval we studied, the E_f and H budgets of the AR were below established thersholds (see Tziotziou et al. 2012; Liokati et al. 2022) which, if crossed, the AR is likely to erupt. The time profiles of the free magnetic energy and helicity resulted from the superposition of two components: (i) A slowly-varying one which was broadly consistent with the evolution of both the total unsigned magnetic flux of the AR and the connected magnetic flux. (ii) Discrete localized peaks of much shorter duration (full widths at half maximum of ~55-160 min). Eight such peaks in each of the E_f and H curves (all well beyond uncertainties) occurred co-temporally with jet events produced in the AR. These local helicity peaks can reasonably be attributed to the jet events because no other type of eruptive activity was registered in the AR. Furthermore, their pairing with E_f localized peaks supports the same conclusion for the origin of the simultaneous E_f peaks.

The jets associated with localized peaks in the E_f and H budgets of the AR are distinguished from the other AR jets by their larger areas of their bases as well as by their longer durations. The former is in line with the fact that E_f and H are extensive quantities. It is interesting, though, that these major jets are also associated with local peaks in the time profiles of the normalized free magnetic energy and helicity parameters.

The free magnetic energy and helicity losses associated with the jets are in the ranges of $(1.1 - 6.9) \times 10^{29}$ erg and $(0.5 - 7.1) \times 10^{40}$ Mx^2, respectively. These values are one to two orders of magnitude smaller than the relevant changes associated with CMEs (see Liokati et al. 2023, and references therein).

Table 1: Free magnetic energy and helicity budgets of jet events.

Event	DE_f		DH	
Number	($\times 10^{29}$ erg)	(%)	($\times 10^{40}$ Mx^2)	(%)
1	-1.9	-57	1.3	-76
2	-1.4	-26	0.5	-40
3	-1.1	-15	1.7	-35
4	-7.9	-27	3.9	-31
5	-3.9	-15	4.0	-27
6	-2.9	-9	5.6	-26
7	-5.5	-18	3.4	-13
8	-6.9	-14	7.1	-34

The derived free energy losses are consistent with the high-end limits of the thermal energy of jets (see Shen 2021). There are no previous explicit reports based on observations about helicity changes directly associated with jets. The percentage losses associated with the jets are significant: 9-57% for the normalized free magnetic energy and 13-76% for the normalized helicity. There is a trend the percentage losses to be larger early on in the evolution of the AR (see Table 1).

This is the first report where changes in the magnetic free energy and helicity budgets of an AR are registered with such clarity with jet activity. Green et al. (2022) were the first to report jet activity in intervals when the helicity index (see Sect. 1) attains large values. In our study the close synchronization of localized E_f and H peaks with jet events allowed us to estimate, for the first time, the free magnetic energy and helicity budgets associated with individual jet events.

More case studies are required to check how often jets may have significant imprints in the evolution of the free magnetic energy and helicity budgets of emerging ARs. As more case studies will be accumulated, it would be interesting to investigate whether the collective E_f and H budgets of such jets are significant. Computations of the field line helicity (e.g. Yeates & Page 2018; Moraitis et al. 2019, 2021, 2024) may also provide insights about the distribution of helicity over the different components of individual jets.

References

Archontis, V. & Hood, A. W. 2008, ApJ, 674, L113
Archontis, V. & Hood, A. W. 2012, A&A, 537, A62
Archontis, V. & Hood, A. W. 2013, ApJ, 769, L21
Bobra, M. G., Sun, X., Hoeksema, J. T., et al. 2014, Sol. Phys., 289, 3549
Couvidat, S., Schou, J., Hoeksema, J. T., et al. 2016, Sol. Phys., 291, 1887
Georgoulis, M. K., Tziotziou, K., & Raouafi, N.-E. 2012, ApJ, 759, 1
Green, L. M., Thalmann, J. K., Valori, G., et al. 2022, ApJ, 937, 59
Gupta, M., Thalmann, J. K., & Veronig, A. M. 2021, A&A, 653, A69
Kusano, K., Maeshiro, T., Yokoyama, T., & Sakurai, T. 2002, ApJ, 577, 501
Linan, L., Pariat, É., Moraitis, K., Valori, G., & Leake, J. 2018, ApJ, 865, 52
Liokati, E., Nindos, A., & Georgoulis, M. K. 2023, A&A, 672, A38
Liokati, E., Nindos, A., & Liu, Y. 2022, A&A, 662, A6
Liu, Y., Welsch, B. T., Valori, G., et al. 2023, ApJ, 942, 27
Moraitis, K., Pariat, E., Valori, G., & Dalmasse, K. 2019, A&A, 624, A51
Moraitis, K., Patsourakos, S., & Nindos, A. 2021, A&A, 649, A107
Moraitis, K., Patsourakos, S., Nindos, A., Thalmann, J. K., & Pariat, É. 2024, A&A, 683, A87
Norton, A. A., Duvall, T. L., J., Schou, J., et al. 2018, in Catalyzing Solar Connections, 101
Pariat, E., Leake, J. E., Valori, G., et al. 2017, A&A, 601, A125
Pariat, E., Wyper, P. F., & Linan, L. 2023, A&A, 669, A33

Pevtsov, A. A., Berger, M. A., Nindos, A., Norton, A. A., & van Driel-Gesztelyi, L. 2014, Space Sci. Rev., 186, 285

Pevtsov, A. A., Canfield, R. C., & Metcalf, T. R. 1995, ApJ, 440, L109

Raouafi, N. E., Patsourakos, S., Pariat, E., et al. 2016, Space Sci. Rev., 201, 1

Schmieder, B., Joshi, R., & Chandra, R. 2022, Advances in Space Research, 70, 1580

Shen, Y. 2021, Proceedings of the Royal Society of London Series A, 477, 217

Shibata, K., Ishido, Y., Acton, L. W., et al. 1992, PASJ, 44, L173

Sterling, A. C., Moore, R. L., Falconer, D. A., & Adams, M. 2015, Nature, 523, 437

Sterling, A. C., Moore, R. L., Falconer, D. A., et al. 2016, ApJ, 821, 100

Sun, Z., Li, T., Wang, Q., et al. 2024, A&A, 686, A148

Thalmann, J. K., Georgoulis, M. K., Liu, Y., et al. 2021, ApJ, 922, 41

Thalmann, J. K., Moraitis, K., Linan, L., et al. 2019, ApJ, 887, 64

Tziotziou, K., Georgoulis, M. K., & Raouafi, N.-E. 2012, ApJ, 759, L4

Wang, Q., Yang, S., Zhang, M., & Yang, X. 2022, ApJ, 929, 122

Wang, Q., Zhang, M., Yang, S., Yang, X., & Zhu, X. 2023, Research in Astronomy and Astrophysics, 23, 095025

Wyper, P. F., Antiochos, S. K., & DeVore, C. R. 2017, Nature, 544, 452

Wyper, P. F., DeVore, C. R., & Antiochos, S. K. 2018, ApJ, 852, 98

Yeates, A. R. & Page, M. H. 2018, Journal of Plasma Physics, 84, 775840602

Yokoyama, T. & Shibata, K. 1995, Nature, 375, 42

Yokoyama, T. & Shibata, K. 1996, PASJ, 48, 353
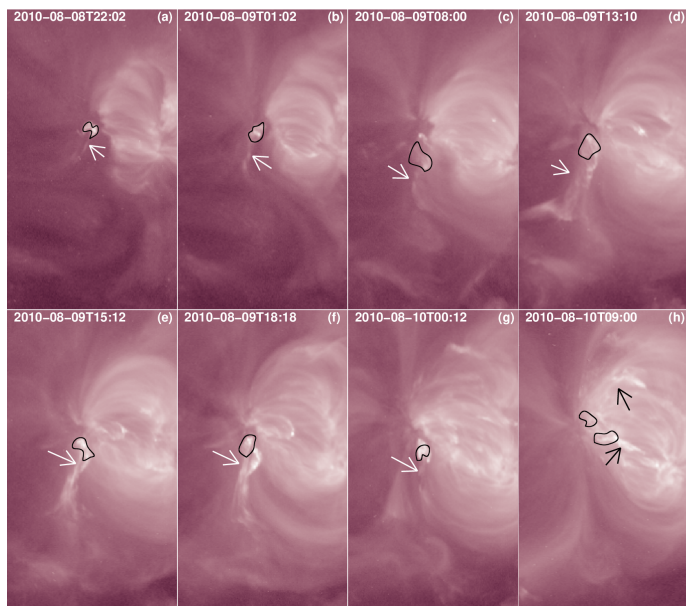
Appendix A: Jets produced in AR11096

Fig. A.1: Selected 211-Å AIA images showing the jets (denoted by arrows) that were associated with localized peaks of the free magnetic energy and helicity budgets of AR11096. Contours outline the calculated apparent areas of the bases of the jets (see text for details). The field of view is $103'' \times 181''$ and corresponds to the black box of Fig. 1. The associated movie is available online.

In Fig. A.1 we show characteristic snapshots of the major jets that were associated with localized peaks of the free magnetic energy and helicity budgets of AR11096. These jet events are marked with arrows. All of the jets that occurred in the AR are marked with arrows in the movie that accompanies the paper. Note that there are two arrows in the bottom right panel of Fig. A.1 due to the presence of two temporally overlapping jet events. All of the jets presented in Fig. A.1 occurred in the eastern part of the AR. In more detail, jets 1 and 2 (see panels a and b) emanated from approximately the same location and the same is true for jets 3-7 (see panels c-g).

The calculations of the apparent areas of the bases of all jets that we detected in AR11096 are presented in panel (a) of Fig. A.2. In each snapshot the jet base area was computed by employing a $35'' \times 35''$ box just below the spire of the jet and by taking into account only the box pixels with intensities exceeding the 2σ levels of their time series above the background (for the snapshots of Fig. A.1 the resulting areas are outlined by the black contours). In addition to this semi-automatic procedure, the bases of the jets were determined by visual inspection. Both methods yielded consistent results (differences of ∼30-40%). The areas that appear in Fig. A.2 result from the average values derived from the two methods. In Fig. A.2 the red symbols correspond to the events displayed in Fig. A.1 while the black symbols corresond to the other jets. Each vertical error bar in the figure denotes the standard deviation of the computed time series of the base area of the jet. When only one image of a jet was available (that was the case for the majority of events) no error bar was attached to our calculation.

In panel (b) of Fig. A.2 we show the duration of the jets. The duration is defined as the interval between the last and first appearance of the jet spire in the AIA images. The duration of jets appearing in only one AIA image has been somewhat arbitrarily set to 2 min (i.e. the cadence of our AIA datacube).
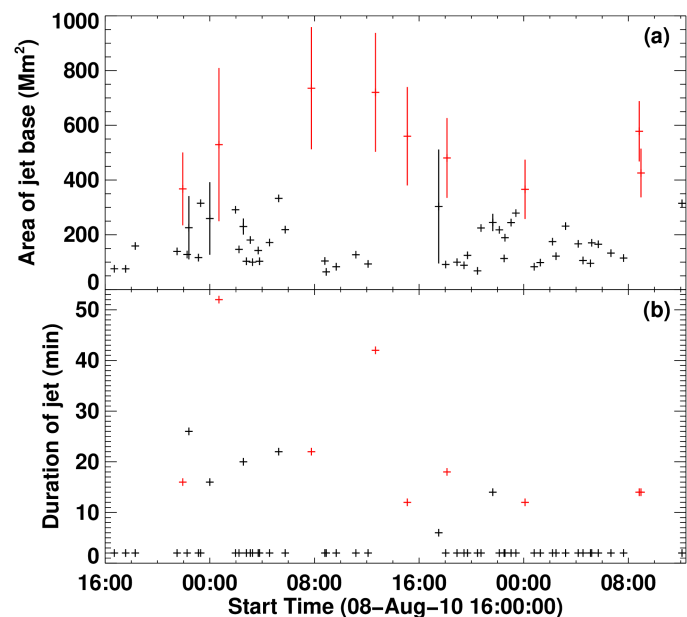

Fig. A.2: (a) Apparent areas of the bases of all jet events that we detected in AR11096. When possible the measurements are accompanied with their uncertainties (see text for more details). (b) Duration of jets. The duration of those jets that appeared in only one AIA image has been set to 2 min. In both panels red symbols correspond to the events presented in Fig. A.1 while black symbols are used for the other events. In both panels each symbol has been placed at the start time of the corresponding jet.